SPATIAL DISTRIBUTION AND GEOMETRICS OF ORIENTALE SECONDARY CRATER. Dijun Guo[1, 2, 3], Jianzhong Liu[1,2], James W. Head[3], [1]Center for Lunar and Planetary Science, Institute of Geochemistry, Chinese Academy of Sciences, 99 Lincheng West Road, Guiyang 550051, China (liujianzhong@mail.gyig.ac.cn). [2]University of Chinese Academy of Sciences, Beijing 100049, China. [3]Department of Earth, Environmental and Planetary Sciences, Brown University, Providence, RI 02912 USA (james_head@brown.edu).

Introduction: The Orientale impact basin is widely accepted to be the youngest impact basin on the Moon. Its well-preserved structures make it a uniqueobject to study the cratering process and initial post-impact modification. Numerous geological [1-5], geophysical [6-8] and impact simulation [9-11] studies have been carried out to assess its characteristic multiring structure, topography and gravity characteristics, ejecta facies, post-basin maria emplacement, all providing insight into the basic process of lunar impact basin formation and evolution. Secondary craters, formed from high-velocity ejecta blocks and debris impacting during the excavation stage of the cratering event, are an important facies in craters and basins [12, 13]. We undertook a comprehensive study of secondary craters of the Orientale basin in order to assess components of the basin ejecta emplacement process that have not been thoroughly investigated previously. In addition, information from the Orientale basin can help identify secondary craters of older and more degraded basins. Two important aspects of basin secondary craters are 1) their spatial distribution, which relates to the power law of impact and 2) their geometrics (morphology and morphometry) which are of critical to the ability to distinguish secondaries from primaries.

We identified 1301 Orientale secondary craters in the range of radial distance up to 6 basin radii from the Cordillera rim and in an azimuth range from 286° to 333° from the Orientale center, a regional where they are the highest abundance of secondaries occurs. Secondary crater diameters range from 1.5 kilometers to 26.4 kilometers. Eithty-four craters that have relatively well preserved structures were selected to conduct a geomectrics study; their diameters range from 4.92 kilometers to 20.53 kilometers.

Data and methods: We used LROC WAC images (100 m/pixel) and the LOLA DEM (29 pixel/degree) to identify secondary craters. For cases where the geologic context is complicated and the identification is not robust, Kaguya images (20 m/pixel) were used.

Criteria for the recognition of a secondary crater have been proposed by various workers (e.g., [14-16]). We follow the criteria established by previous analyses: 1) crater is entrained within a chain, elongate crater group, and/or has a "herringbone" ejecta pattern; 2) shallower than primary impact craters; 3) highly elliptical with the long axis radial to the Orientale basin center; 4) contains numerous interference features such as septa and mounds. An additional note for criteria 3 is that with decreasing secondary crater size, the shapes are more subcircular.

Recognition and measurement of the secondary craters are made on ESRI ArcMap using Crater Helper Tools (http://astrogeology.usgs.gov/facilities/mrctr/gis-tools). The geometrics are computed by in-house scripts basiclly follow the steps of [17] with small modifications. For each crater, a LOLA DEM (29 m/pixel) with 10 radii height and 10 radii width is created and is apllied with azimuthal equidistant projection to the crater center. Before measuring the geometrics, the DEM is detrended by a plane fitted from pixels at the ring of 3 and 3.5 radii to remove large topographic gradients, and then redetrended by a plane fitted from global maxima (the max elevation of a profile from crater center to 2.5 radii) of the first detrended DEM. Thereafter, three types of interest points including slope break, local maxima and global maxima are extracted from 512 evenly spaced profiles [17]. Based on the points of interest, the crater rim is traced out, and is fitted with an ellipse and circle (Figure 1). The crater geometrics are calculated through profiles that start from crater center through rim pixels to the edge of the image.

For each crater, 47 metrics and related attributes are measured, including all metrics of [17] except cavity volume. Part of these metric results are reported here.

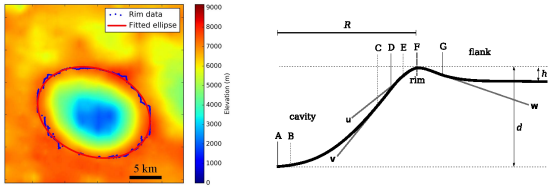

Figure 1. Left: a traced crater rim and its ellipse fit in red. The crater diameter is 16.3 km on average. Right: reference locations for metrics measurements (revised from [17]), in which A and B are separated by radial distance 0.1R, as are C and D, D and E, as well as E and F. F and G are separated by a distance 0.2R.

Spatial distribution: The secondary crater study region is divided into 12 annuli with widths equal to half of Orientale radius (232.5 km). The statistics in each annulus are shown in Figure 2. The average crater diameter decreases with increasing distance from the Orientale basin, and the maximum diameter also decreases with increasing distance (Figure 2, a). As shown in Figure 2 (b), secondary craters are concentrated in annuli from 1 to 3.5 radii; although annuli at 3.5 radii has the largest secondary crater count, the largest density is located at 1.5 radii annulus sector.

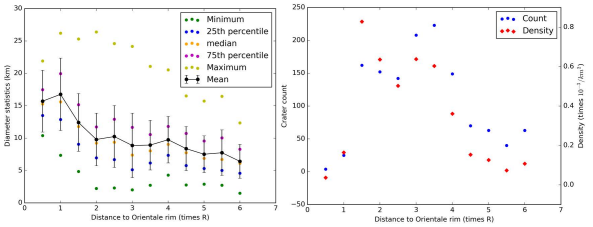

Figure 2. Spatial distribution of Orientale secondary craters (a). Secondary crater count and density in different anuuli (b). Errorbar of mean value in (a) represents the standard deviation. X axis is the distance of annulus to Cordillera ring, normalized to the Orientale radius.

Geometrics: Because the geologic context is complex and the substrate is diverse, and secondary craters are more complex than primaries, not all of the 84 selected craters have a good rim trace and robust measurement results. Sixty craters with the most reliable results were chosen to conduct a final analysis. All the metrics for a single crater is an average of all profiles along the trace from crater center through every extracted rim pixel and beyond.

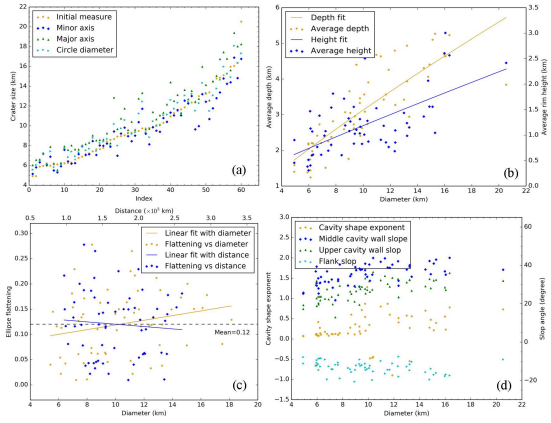

Figure 3. Geometrics of Orientale secondary craters. (a) crater size using different measurement techniques, including initial estimate by Crater Helper Tools, ellipse fit and circle fit. (b) crater average rim to floor depth and rim height and their power law fits. (c) the fitted ellipse flattening versus crater diameter and distance to Orientale center and their linear fits. (d) cavity shape exponent and cavity and flank slope degree versus diameter.

Figure 3 (a) shows that the ellipse fit and the circle fit can provide a reasonable crater size estimate. However, rim fitting results in a slightly larger crater size, as seen in the figure. The average value of initial diameter is 9945.3 meters, while the average cirlce fit diameter is 10260.2 meters and average ellipse fit diameter is 10325 meters (sum of semi major and semi minor axis). Given that the fit process is based on the rim positions and more dots on the rim contribute to the final results, we suggest the fitted diameters are more reliable. On the other hand, the incident angle of image has an influence on manual crater rim identification [18] .

To remove the context and background topography, the global topography is detrended based on the plane formed by the topography of all rim pixels before extracting depth, and each profile is detrended individually (based on pixels beyond 2 radii on the profile) before estimating the rim height. Both rim to floor depth and rim height increase with diameter, but the depth has a larger slope than the height, as shown in Figure 3 (b). A power law fit indicates that depth (d) and diameter (D) follow the relation $d=0.454\times D^{0.839}$, while height (h) and diameter follow the relation $h=0.143\times D^{0.929}$, all in km.

One important charateristic of secondary craters is their elliptical shape. Figure 3 (c) shows the change in ellipse flattening versus crater diameter, and distance to the Orientale basin. The mean value of flattening of the selected craters is 0.12. Secondary crater flattening decreases with increasing distance to the primary crater but increases with an increase of crater diameter, which meets the expectation that futher located secondary craters are formed in larger impact angles and larger secondaries are more concentrated in closer distance.

Figure 3 (d) shows some metrics of crater section. The cavity shape exponent, which is the exponent of the power law fit to a radial profile from B to E (Figure 1), does not show any apparent trend with increasing diameter but changes significantly with changes in topographic context. The middle cavity wall slope, which is the slope angle of a line fitted from C to E (Figure 1, line v), the upper cavity wall slope, which is the slope angle of a line fitted from D to F (Figure 1, line u), and the flank slope angle, which is the slope angle of a line fitted from F to G (Figure 1, line w), all show little trend with diameter, indicating relatively constant values with crater size.

Summary: We investigated the secondary crater spatial distribution from 1301 identified Orientale secondaries, and the geometrics from 60 selected secondary craters whose shapes can be documented. The largest secondary crater diameter is 26.4 kilometers, ~2.8% of Orientale basin diameter. Secondary craters are concentrated distributed in an area of 1 to 3.5 primary radii outward from the Orientale rim crest (the Cordillera Mountain ring), especially in the 1 to 1.5 radii region. The secondary crater rim ellipse shape has a mean flattening value of 0.12, and it decreases with crater diameter, and increases with the distance to the primary. The cavity shape exponent varies when the diameter is >10 km, while cavity and flank slope values are almost independent of crater size.

References: [1] Head, 1974, *The Moon*, 11, 327. [2] Scott & McCauley, 1977, *I-1034*. USGS. [3] Moore et al.,1974, *LPSC V*, 71. [4] Spudis et al., 1984, *JGR,* 89, C197. [5] Head, et al., 1993, *JGR,* 98, 17149. [6] Booker, 1970, *Natur,* 227, 56. [7] Vonfrese, et al., 1997, *JGR,* 102, 25657. [8] Zuber, et al., 2016, *Sci*,354, 438-441. [9] Johnson, et al., 2016, *Sci*, 354, 441. [10] Potter, et al., 2013, *JGR,* 118, 963. [11] Wieczorek & Phillips, 1999, *Icarus,* 139, 246. [12] Collins et al., 2012, *Elements,* 8, 25. [13] Pike & Wilhelms,1978, *LPSC IX*, 907. [14] Shoemaker, 1962, *Interpretation of lunar craters*. Academic Press. [15] Wilhelms, 1976, *LPSC VII*, 2883. [16] Robbins & Hynek, 2014, *EPSL* , 400, 66. [17] Watters, et al., 2015, *JGR,* 120, 226. [18] Gault & Wedekind,1978, *LPSC IX*, 3843.